Fermi National Accelerator Laboratory

TM-1455
2281.000

Single Wire Drift Chamber Design

J. Krider

Fermi National Accelerator Laboratory
P.O. Box 500
Batavia, IL 60510 USA

March 30, 1987

Operated by Universities Research Association Inc. under contract with the United States Department of Energy

30 March 87

Single Wire Drift Chamber Design

J. Krider
Research Facilities Department

This report summarizes the design and prototype tests of single wire drift chambers to be used in Fermilab test beam lines. The goal is to build simple, reliable detectors which require a minimum of electronics. Spatial resolution should match the 300 μm rms resolution of the 1 mm proportional chambers that they will replace. The detectors will be used in beams with particle rates up to 20 KHz. Single track efficiency should be at least 99%. The first application will be in the MT beamline, which has been designed for calibration of CDF detectors. A set of four x-y modules will be used to track and measure the momentum of beam particles.

MECHANICAL DESCRIPTION

One chamber module consists of four independent single wire drift cells, each with an active area of 102 mm by 102 mm. Two cells have vertical wires to measure a horizontal coordinate, and the other two cells have horizontal wires to measure a vertical coordinate. One cell has its anode offset 20.3 mm to one side of the center, while the other cell measuring the same coordinate has its anode offset 20.3 mm to the other side. This resolves the left-right ambiguities and provides a constant monitor of the electron drift velocity.

The various layers of anodes, cathodes, cell isolation foils, and spacers are stacked on alignment pins mounted on a 12.7 mm thick aluminum base plate. Locations of individual anode and cathode planes are maintained to ±25 μm by the pins. All anode planes are interchangeable, with the absolute position accuracy of all anode wires being ±125 μm with respect to the base plate centerline.

There is no gas seal between layers within the detector stack. A removable aluminum box cover bolts to the base plate and has an O-ring gas seal. High voltages and anode signals pass through the base plate using connectors sealed with epoxy. Mylar beam windows of 125 μm thickness cover 102 mm by 102 mm holes in the upstream and downstream aluminum box faces. The air leak rate of the prototype assembly was measured to be

250 cc/hr at 2.0 psig, which corresponds to 5 cc/hr at the likely operating pressure of 1.0 inch of water.

A cell consists of an anode plane centered in a 9.5 mm total gap between a pair of field shaping cathode planes. A 15 μm thick grounded aluminum foil is located 9.5 mm to the outside of each cathode to electrostatically isolate that cell from other cells in the chamber. The crossection of an inside edge of one cell is shown in Figure 1. The various layers have different inside dimensions in order to make the high voltage breakdown path across the insulator surfaces longer than the breakdown path through the gas.

Each anode plane is a single sided printed circuit with the layout shown in Figure 2. It has an 85 μm diameter beryllium copper field wire at either edge of the active area. These field wires are operated at the same potential as the nearest cathode plane field wires in order to improve the linearity of the drift field near the cell boundaries. A single 25 μm diameter gold plated tungsten anode wire is located 20.3 mm to the left of center. A schematic of the circuitry inside the box for one cell is shown in Figure 4. The anode wire is operated at a positive high voltage. The output signal is decoupled from the high voltage with a 1.0 nF 7.5KV capacitor. A 1.0 MΩ resistor in series with the power supply limits the peak charging current to the wire.

The cathode printed circuit layout is shown in Figure 3. The board has solder pads for 51 field shaping wires. Cathode wires are 85 μm diameter beryllium copper spaced 2.03 mm apart. A resistor divider network on the board supplies the required potential distribution. The voltage divider uses two 1.00 MΩ 1/4 watt 1% metal film resistors in series per field voltage increment. For a drift field gradient of 1000 V/cm, the voltage across each resistor is 100 V. The divider current is 100 μA, which is 10,000 times the average current draw of the chamber in a 20 KHz beam. The five field wires nearest to the anode are isolated from the divider by 1.00 MΩ series resistors to limit the discharge current from the decoupling capacitor in the event of a high voltage breakdown.

ELECTRONICS

The chamber amplifier/discriminator used for the prototype studies was designed at Indiana University in 1975.[1] Figure 5 shows the

circuit schematic for the 16 channel card. The input impedance is 570 Ω. The circuit uses three stages of ECL 10116 differential receivers, which are DC coupled in series for an overall gain of approximately 750. The input offset of each channel is trimmed with a potentiometer. The inputs are protected from large pulses by diodes. The inputs of three channels use the three receivers of one IC for the lowest voltage amplification stage. Separate IC's are used for intermediate and high level amplification to minimize stray feedback. As the input threshold is lowered to zero, the output goes through the transition from low to high state without oscillation. The sensitivity of input threshold to power supply voltage is 0.5 μA/V. The temperature coefficient of the threshold is 4.0 nA/°C. A new four channel PC board is being prepared.

Time slewing of the amplifier was measured with a pulse generator and a series of attenuators. The amplifier was set to a threshold of 4.0 μA, and the input to output delay was measured for different amplitude input pulses. Figure 6 shows that the variation in delay, or time slewing, is 7 ns for an input range of 2 to 20 times threshold. This computes to a drift position measurement error of 450 μm in a chamber using a 50% argon - 50% ethane gas mixture and a 1000 V/cm drift field. However, this error will be much smaller in practice, because the spread in chamber pulse heights will be only a factor of two.

EFFECTS OF CABLING ON TIME RESOLUTION

Measurements of amplifier time slewing were also made using chamber signals from a Ru106 source. The gas mixture was 90% argon - 10% carbon dioxide. The amplifier output was split into two paths. One path went directly to a discriminator to generate a TDC start signal. The discriminator threshold of 50 mV was only 6% of the maximum pulse height, so it accounted for a small fraction of the slewing, which was caused by slow risetimes.The other amplifier output traveled through either 130 ft or 395 ft of RG108 twinax cable before generating the TDC stop. The time distributions are shown in Figure 7a, with the chamber operating at the edge of its high voltage efficiency plateau, and in Figure 7b, 100 V onto the efficiency plateau. For 130 ft of cable the time slewing is 25 ns FWHM at the edge of the plateau and 6.3 ns FWHM 100 V onto the plateau. For 395 ft of cable the results are 16 ns and 4.8 ns. Time slewing

is smaller with the longer cable, because the cable attenuates the leading edge of the faster risetime signals more strongly, thus bunching the risetime spectrum. The production system will use Twist-n-Flat cable with the longest run to signal repeaters being 150 ft. This cable has a risetime comparable to the 395 ft of twinax used in the above measurements.

The risetimes to the ECL crossover voltage were measured to be 15 ns for 350 ft of twinax, 7 ns for 100 ft of Twist-n-Flat as shown in Figure 8, 21 ns for 200 ft of Twist-n-Flat, and 40 ns for 300 ft of Twist-n-Flat. The shallow voltage slope at ECL crossover obtained with long cables makes the system timing more sensitive to noise. Figure 9 presents an example of the amount of time measurement error introduced by 100 mV p-p of differential noise as a function of Twist-n-Flat cable length; 15 ns of drift time corresponds to about 1 mm of drift distance. Photographs of chamber signals at the end of 100 ft of Twist-n-Flat are shown in Figure 10a for a Ru106 source at the plateau edge (1517 V) and 100 V onto the plateau, and in Figure 10b for Fe55 signals at the same high voltages.

CHAMBER PERFORMANCE

The chamber gain as a function of high voltage was measured by varying the amplifier threshold and determining the corresponding anode high voltage which produced 50% efficiency. Efficiency was measured with respect to tracks through a pair of scintillation counters. Figure 11 shows the test setup. The gas mixture was 50% argon - 50% ethane. Results are presented in Figure 12 for the threshold range of 1 to 3 μA. The slope is approximately a factor of two gain change per 90 V.

Figure 13 shows typical high voltage efficiency and anode singles count rate plateaus for 50% argon - 50% ethane and an amplifier threshold of 2.0 μA. The efficiency rises from zero to maximum with about 200 V change in the high voltage. Using the chamber gain factor determined above, this suggests that the chamber pulse height spectrum for Ru106 has a full width of about a factor of five, i.e., the maximum pulse height is five times the minimum pulse height. The efficiency rises from 10% to 90% in 120V, a spread of 2.3 in pulse height. The spectrum has a narrower width for minimum ionizing beam tracks.

The plateaus of three different cells were studied using 50% argon - 50% ethane and a 2.0 μA threshold. For Ru106 tracks passing close to each anode the 50% efficiency point varies by only 6 V. Based on this measurement all four cells within a module will be operated at the same anode high voltage from a single power supply. The shift in plateau was studied for a 6 cm drift (7 cm is the maximum possible) compared to essentially zero drift. For the two cells with 2 mm field wire pitch the 50% efficiency point shifted upward by an average of 20 V, indicating a loss of about 15% of the primary electrons. For the third cell, which was modified to have 4 mm field wire pitch, the plateau shifted 55 V, indicating a loss of about 35% of the primary electrons. For this reason 2.0 mm field wire pitch will be used in the production chambers.

Figure 14 shows the drift velocity in 50% argon - 50% ethane as a function of the drift field. Drift velocity saturation sets in at about 450 V/cm; however, the velocity continues to increase gradually with increasing field. Drift velocity is approximately 5.5 cm/μs at 500 V/cm. The production chambers will operate with a drift field of approximately 1000 V/cm.

A typical drift time spectrum for cosmic ray tracks using a gas mixture of 90% argon - 10% carbon dioxide is shown in Figure 15; the drift field is 570 V/cm. The average drift velocity is 2.0 cm/us.

The linearity of drift velocity in the vicinity of an anode wire was studied with cosmic rays by comparing the measured drift time in cell 2 to the predicted drift time based on the measured drift times in cells 1 and 3. The cell 2 anode is on the opposite side of the detector centerline from the cell 1 and 3 anodes; therefore, most tracks near anode 2 are much farther from anodes 1 and 3 and are in the linear region of those cells. Scatter plots were made for the measured cell 2 drift time vs. the expected drift time calculated from the average of the drift times in cells 1 and 3. Figure 16 is for 50% argon - 50% ethane at 770 V/cm, while Figure 17 is for 90% argon - 10% carbon dioxide at 570 V/cm. The scattering of background points is caused by left-right ambiguities which the analysis program is not sophisticated enough to resolve correctly. The argon - ethane mixture clearly has much better linearity. Argon - carbon dioxide produces nonlinearity over a region of at least ±1 cm around the anode wire. Argon - ethane will be used in the production chambers.

Time resolution studies were done with both of the previously

mentioned gas mixtures. The time resolution is presented in the figures as the difference between the measured drift time for cell 2 and the calculated drift time for cell 2 using measured drift times from cells 1 and 3. These resulting drift time "error" distributions include both the error from cell 2 and the error from the calculated drift time. Let σ(cell) be the rms measurement error per cell. The rms error of the calculated drift time is then $\sigma(\text{cell})/\sqrt{2}$, since the calculation involves the average of two uncorrelated measurements. The σ(total) of the distributions in the figures is the sum in quadrature of σ(cell) and $\sigma(\text{cell})/\sqrt{2}$. Thus $\sigma(\text{cell}) = 0.82\sigma(\text{total})$.

Cosmic ray data for the entire active area of the detector using 50% argon - 50% ethane are presented in Figure 18. The horizontal scale is 1.38 ns/bin. The FWHM of this distribution is:

(16 bins)(2 TDC counts/bin)(35 μm/ count) = 1120 μm

The global resolution per cell is then σ = 390 μm. This value should improve for beam tracks, which are all nearly normal to the cells. A similar cosmic ray measurement with 90% argon - 10% carbon dioxide is shown in Figure 19. It has a long tail caused by the nonlinear drift velocity. The horizontal scale is 2.5 ns/bin

Another resolution measurement using the argon - carbon dioxide mixture and a well collimated Ru106 source, and requiring that the analyzed events all have cell 2 in the single TDC count 1190, is shown in Figure 20. The horizontal scale is 12.5 ns/bin. This localized measurement yields a resolution per cell of 380 μm, but to take advantage of this resolution, a correction would have to be applied for the variation in drift velocity across the cell.

CHAMBER GAP STUDY

When the chamber operates with a non-saturating gain, the anode pulse risetime is equal to the spread in drift times of the electrons from the initial ionization track. The following assumptions were used to produce a simplified model of the relative drift times from different points along the ionization track: (1) the track is normal to the chamber, (2) the drift path is parallel to the midplane of the chamber until the last

5 mm of cell length from the anode, at which point the electron turns abruptly toward the anode, and (3) the drift velocity is constant at 5 cm/μs. The resulting drift time distribution predicted by this model is presented in Figure 21. For the chamber described in this report, with an anode to cathode gap of 5 mm, the electrons arrive at the anode over a period of 42 ns.

When the chamber is operating at the edge of its high voltage efficiency plateau for a given particle, ionization must be collected from the entire ±5 mm path length in order to saturate the amplifier output. The amplifier has a linear gain response for input signals between zero and 2 μA, and typically operates with a threshold of 2 μA. Thus a pulse with a risetime of 42 ns is produced. If the chamber signal is increased by a factor of two, either by raising the high voltage 90 V or by having a more strongly ionizing incident particle, then the amplifier will saturate with the charge collected from the central ±2.5 mm (the shortest drift distance) and will have a risetime of only 12 ns.

In the case of Ru106, which produces tracks with a total spread of 5x in primary ionization, the model predicts a time spread of 40 ns full width at the edge of the plateau or 10 ns full width 100 V onto the plateau. These predicted values are close to the measured values in Figures 7a and 7b, with the longer measured tails probably being produced by inclined tracks.

For a 10 mm long minimum ionizing track the average number of primary electrons produced is 30, so the pulse height distribution will have an rms width of 18%. Under these conditions the model predicts a time spread of 6.0 ns rms at the plateau edge or 3.5 ns 100 V onto the plateau. Figure 22 shows the calculated time spread as a function of the anode to cathode gap, when the chamber is operating 100 V onto the plateau. A gap of 9.5 mm has been chosen, with the time slewing condition setting the upper limit, and general ease of mechanical construction setting the lower limit. The chamber will operate 100 V onto the plateau.

The contributions to overall chamber resolution include (1) gas diffusion, (2) the spread in drift path length described above, and (3) electronics time slewing. Gas diffusion contributes 260 μm rms for the maximum drift of 7 cm, or 140 μm rms form a typical 2 cm drift.[2] The drift path length variation contributes 3.5 ns = 190 μm rms. Amplifier slewing contributes 3.7 ns = 200 μm rms. When these factors are added

in quadrature the overall resolution is predicted to be 380 μm for a 7 cm drift or 310 μm for a 2 cm drift. The measured values for cosmic rays are consistent with these predictions.

REFERENCES

[1] R. R. Crittenden, S. C. Ems, R. M. Heinz and J. C. Krider, Nucl. Instr. and Meth. 185 (1981) 75-79.

[2] A. Piesert and F. Sauli, CERN 84-08 (1984).

LIST OF FIGURES

Figure 1. Crossection of the edge of a cell

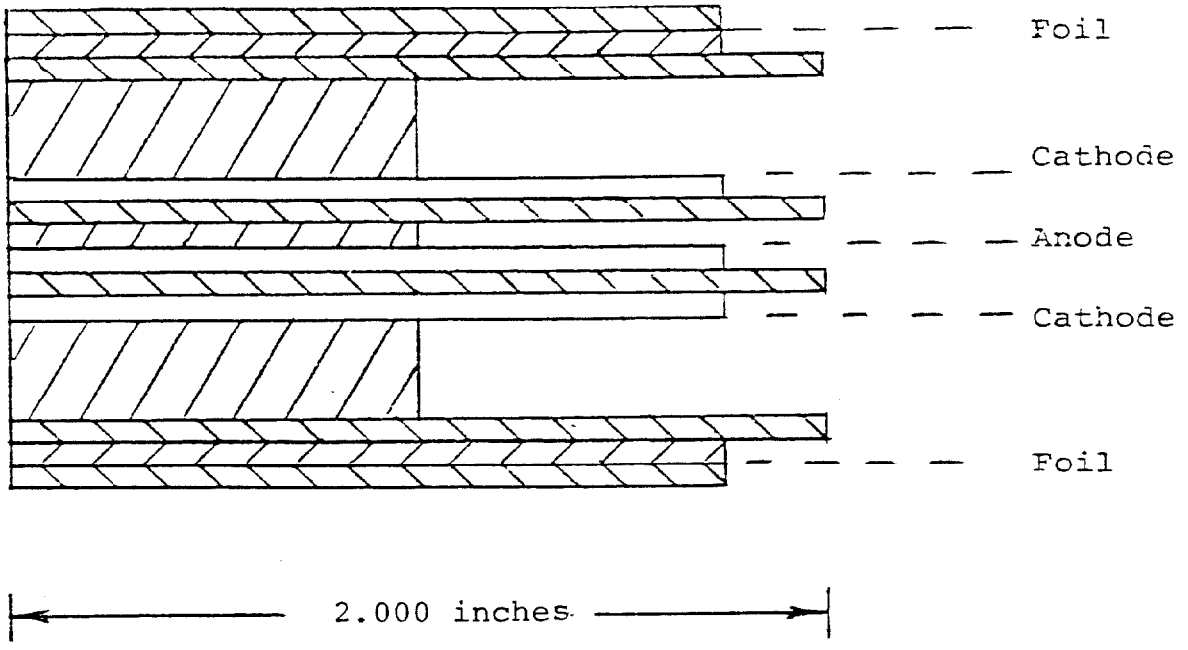

Figure 2. Anode printed circuit

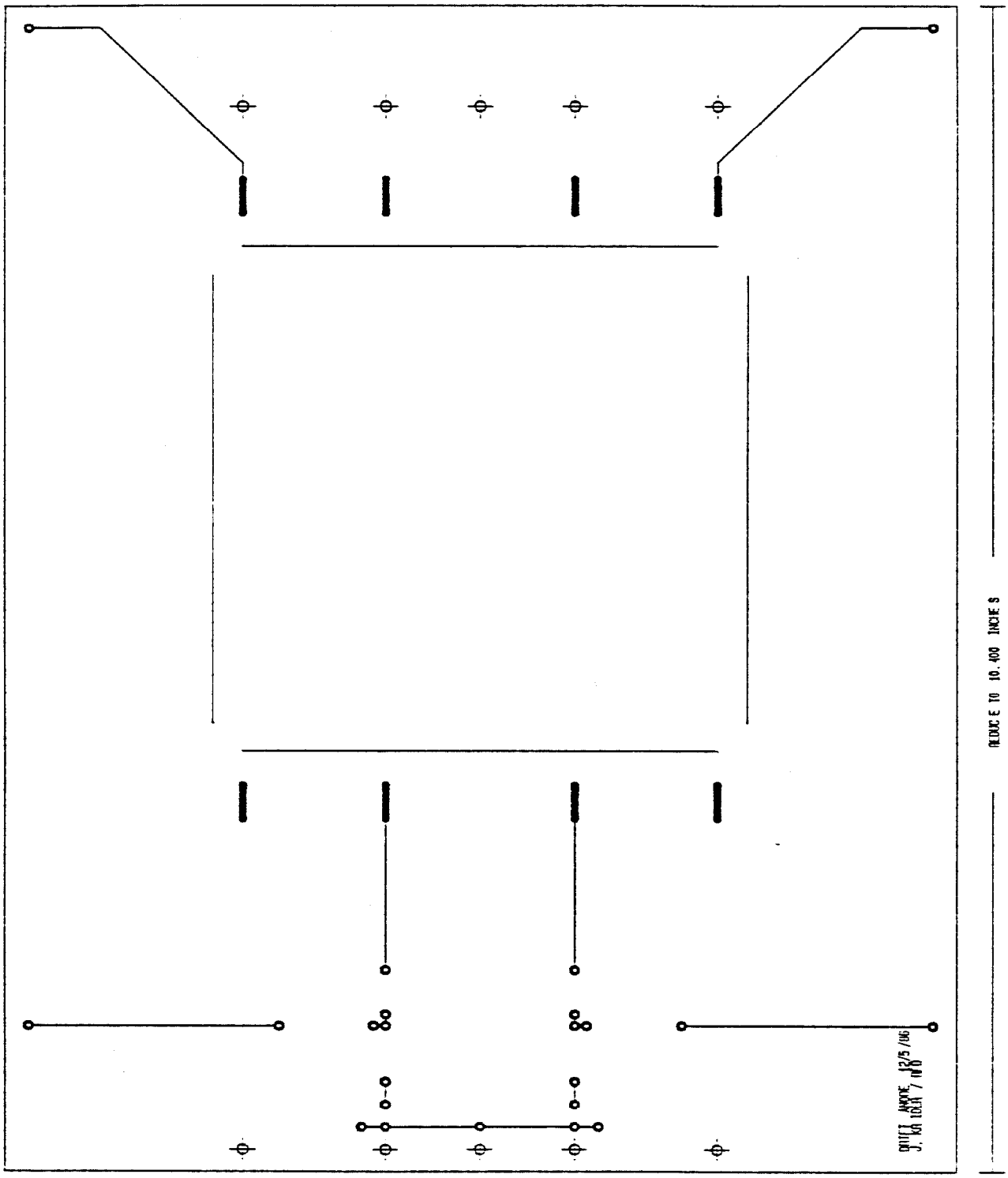

Figure 3. Cathode printed circuit

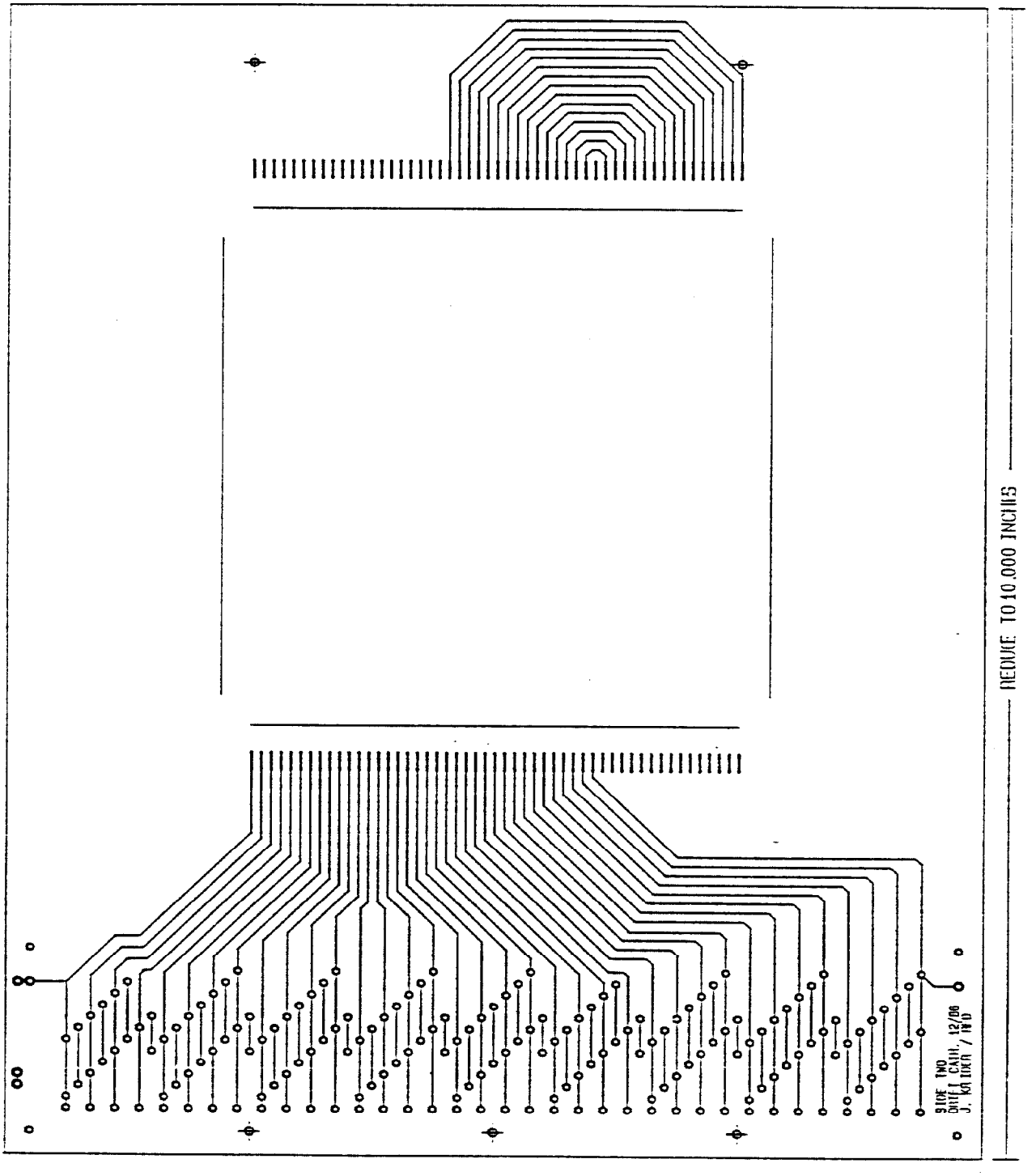

Figure 4. Circuit diagram for one cell

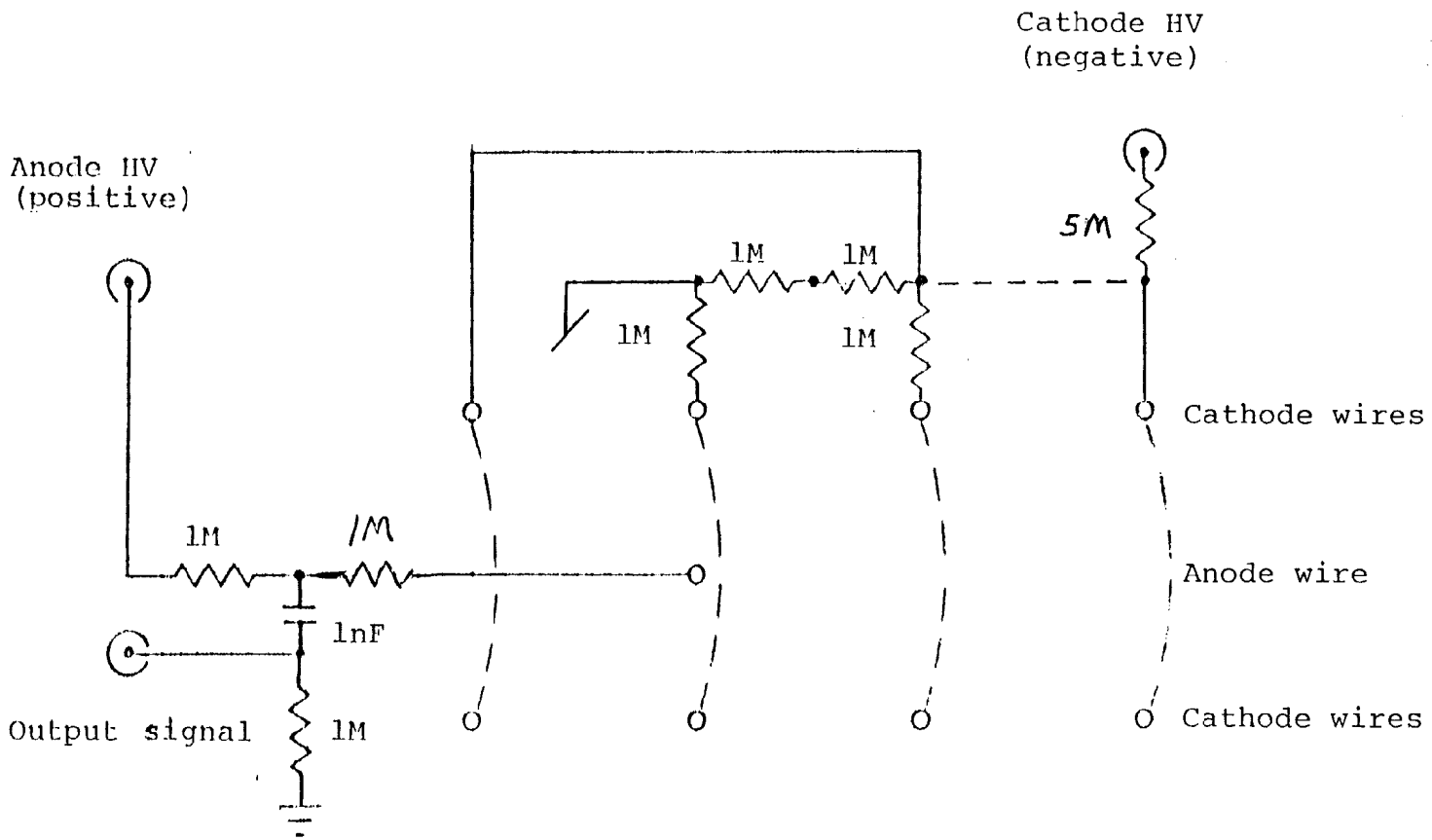

Figure 5. Chamber amplifier schematic

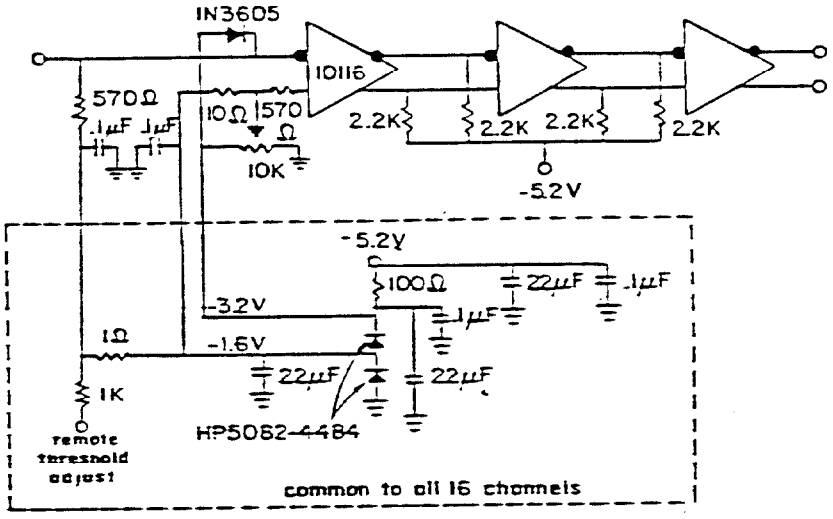

Figure 6.

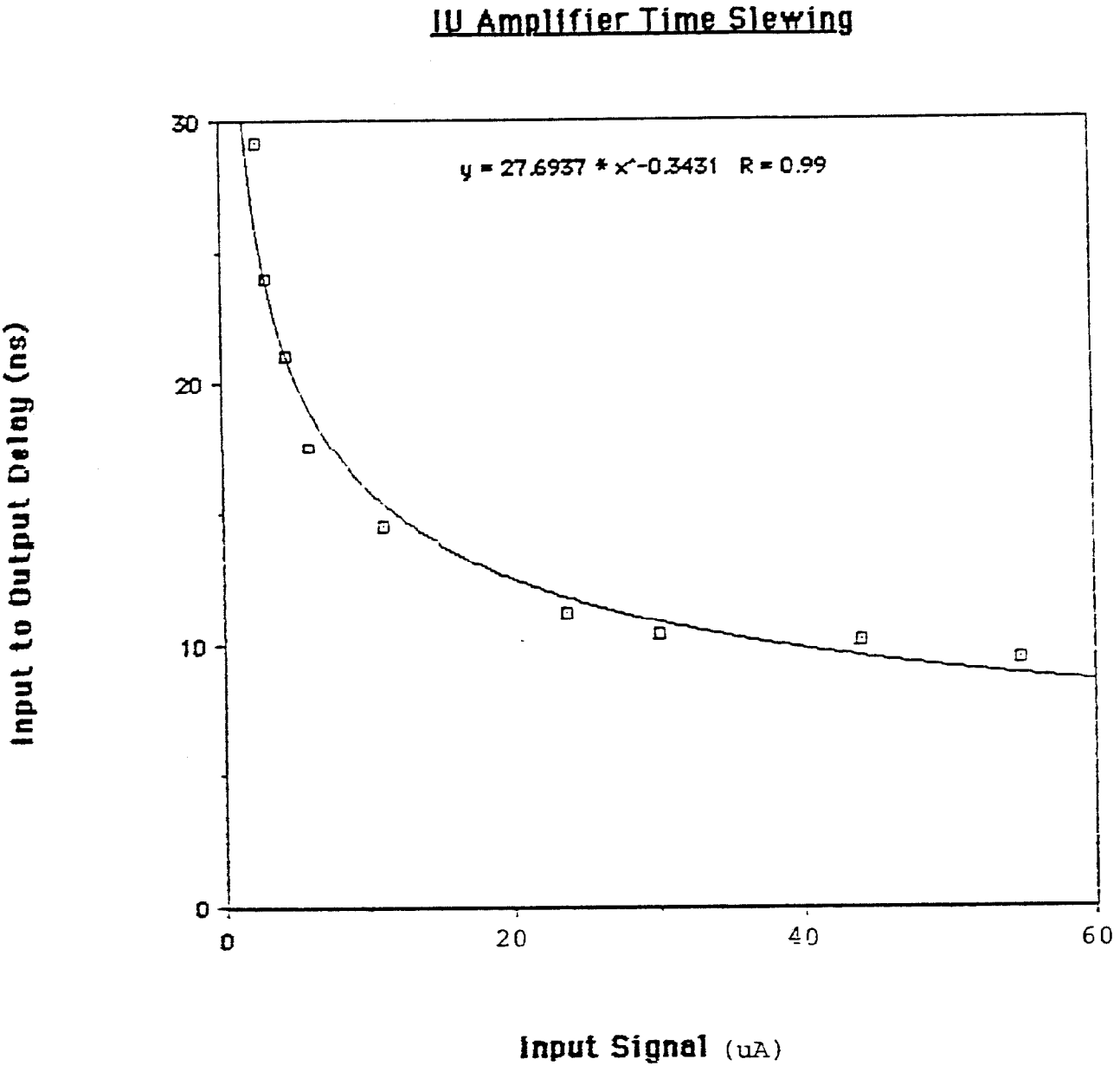
IU Amplifier Time Slewing
y = 27.6937 * x^-0.3431 R = 0.99
Input to Output Delay (ns)
30
20
10
0
0
20
40
60
Input Signal (uA)

Figure 7a. Time slewing for signals at the plateau edge

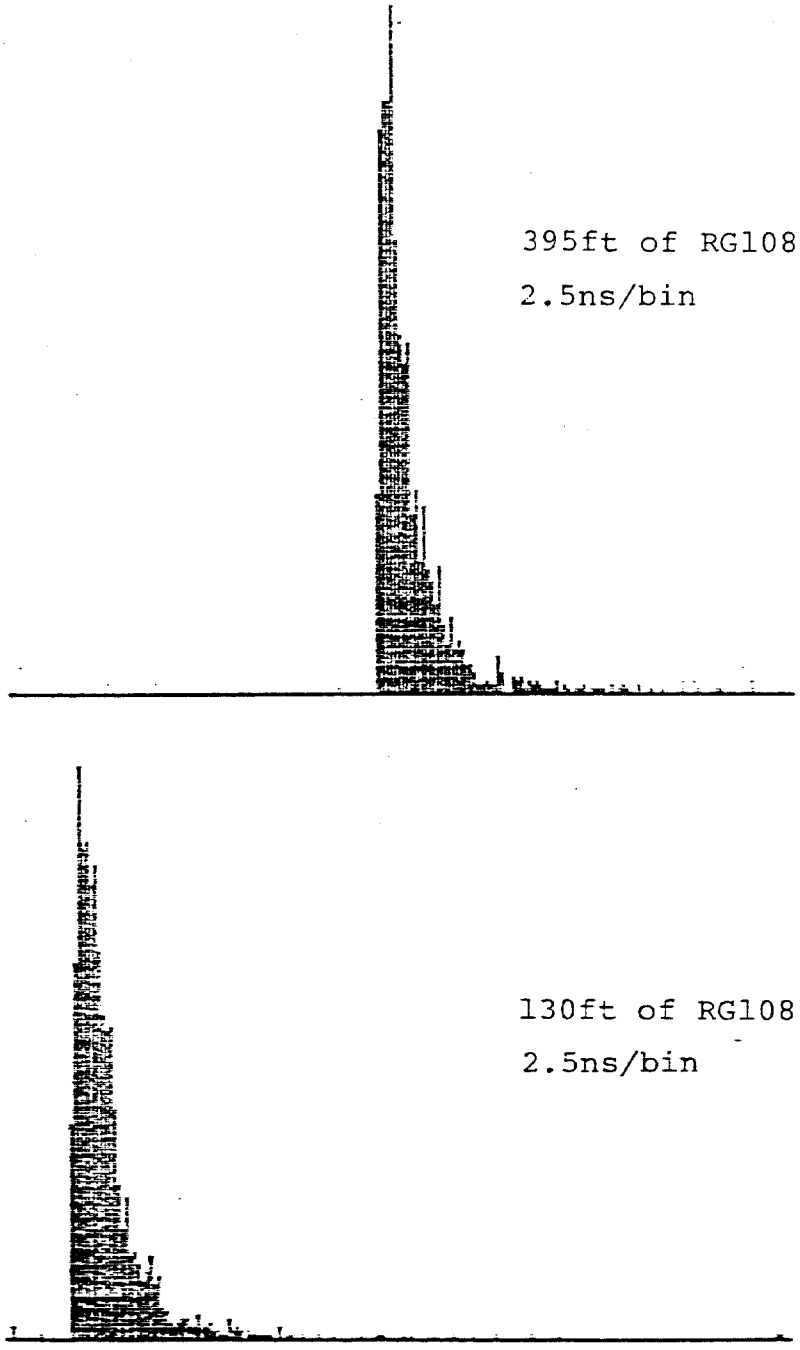

Figure 7b. Time slewing 100V onto the plateau

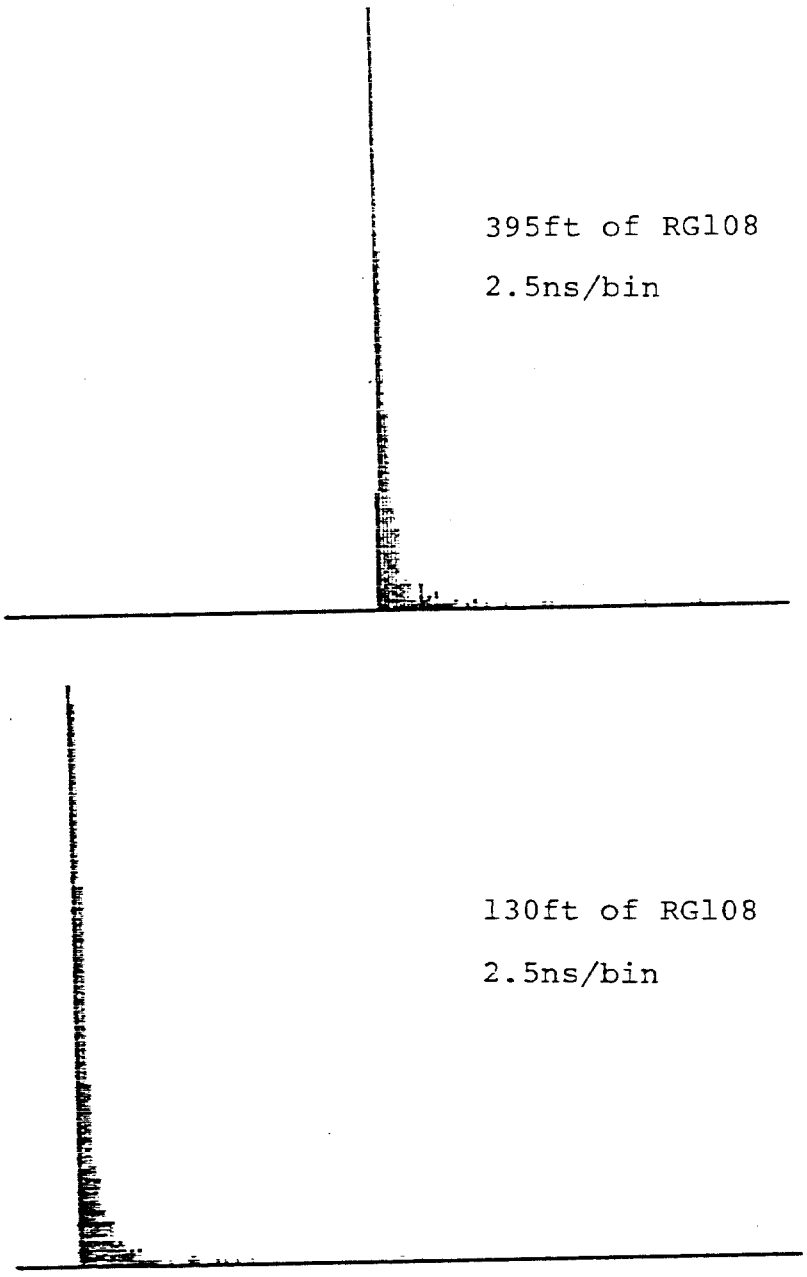

Figure 8. ECL signals after 100ft of flat cable

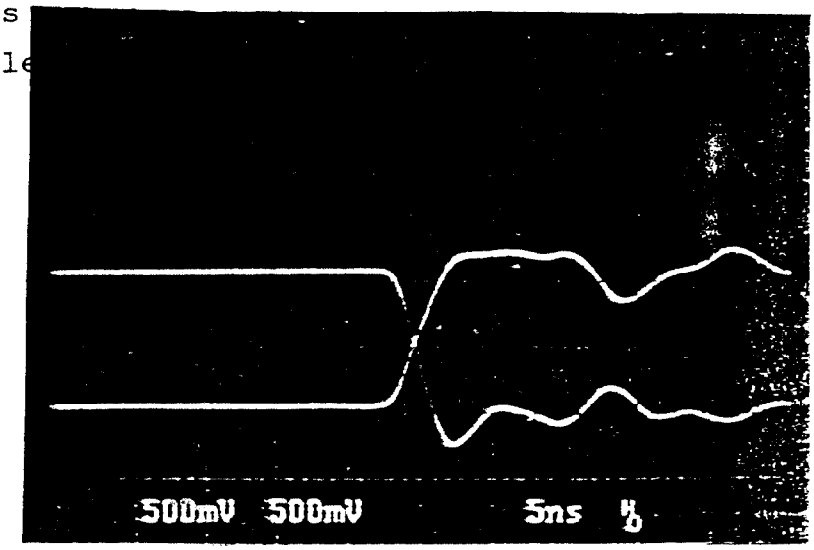

Signal into cable

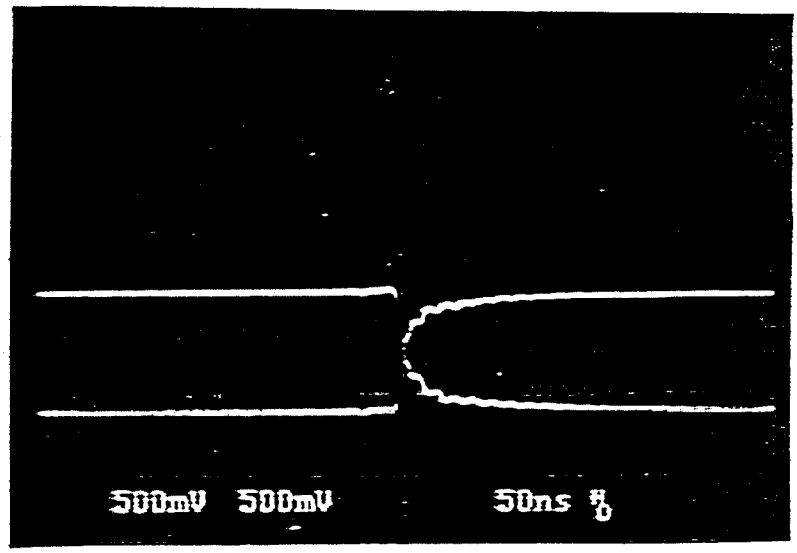

Cable output 50ns/div

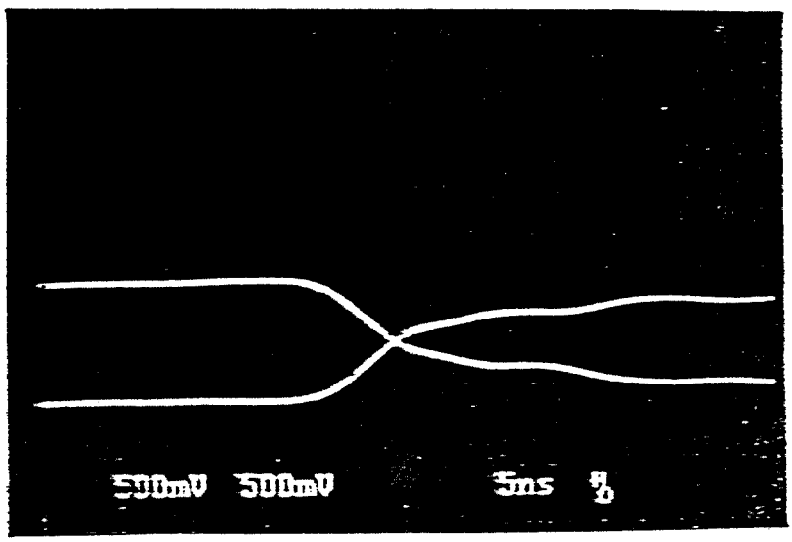

Cable output 50ns/div

Figure 9.

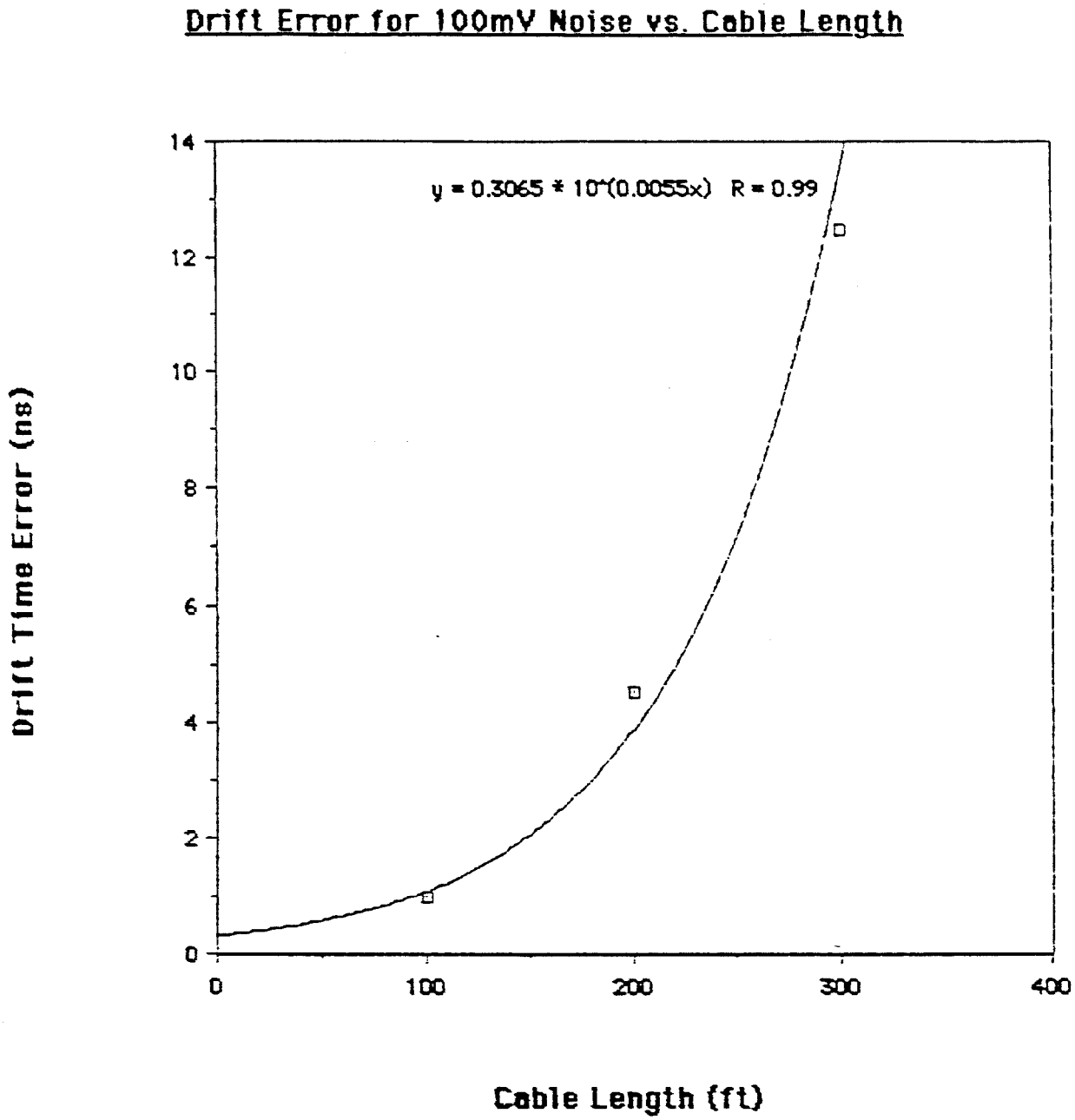
Drift Error for 100mV Noise vs. Cable Length
y = 0.3065 * 10^(0.0055x) R = 0.99
Drift Time Error (ns)
Cable Length (ft)
0
2
4
6
8
10
12
14
0
100
200
300
400

Figure 10a. Ru106 signals after 100ft of flat cable

At plateau edge
(1517V)

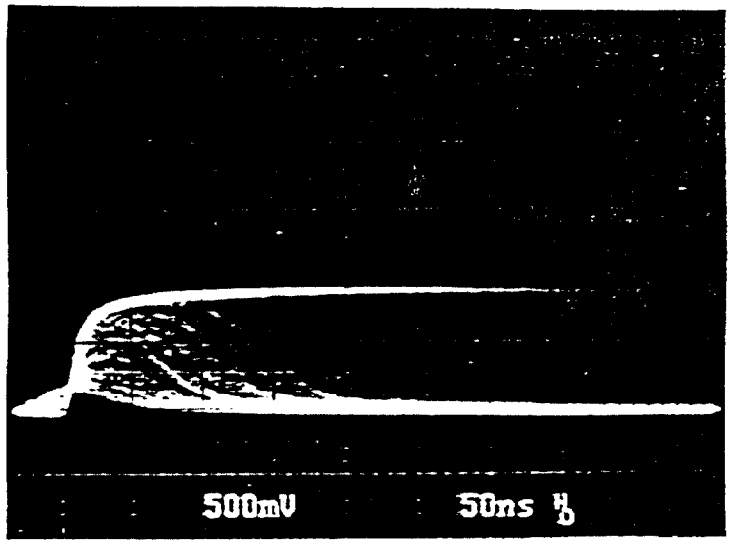

100V onto plateau
(1620V)

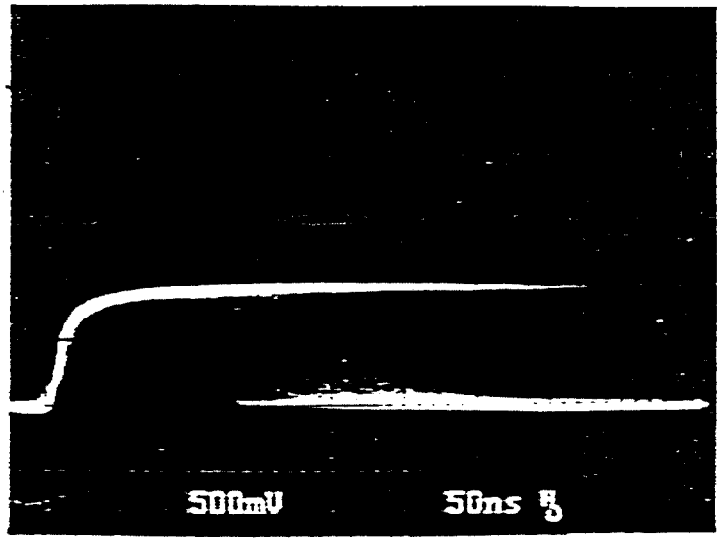

Figure 10b. Fe55 signals after 100ft of flat cable

At 1517V

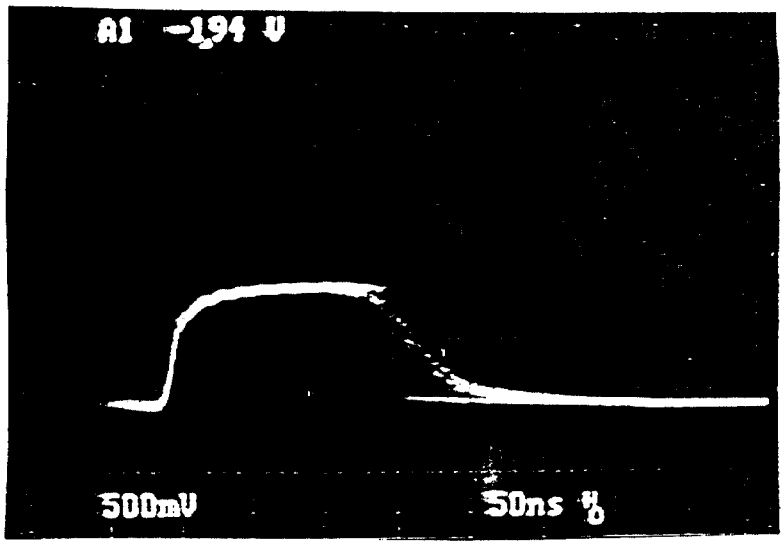

At 1620V

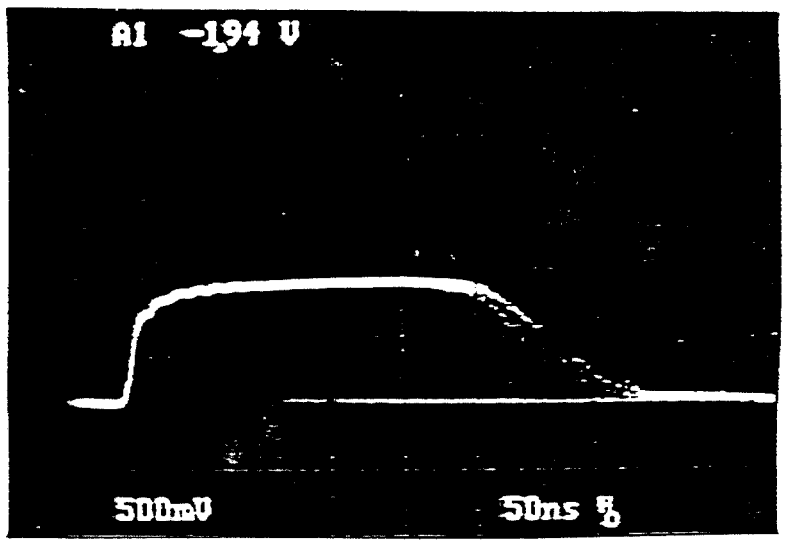

Figure 11. Efficiency and drift time measurement setup

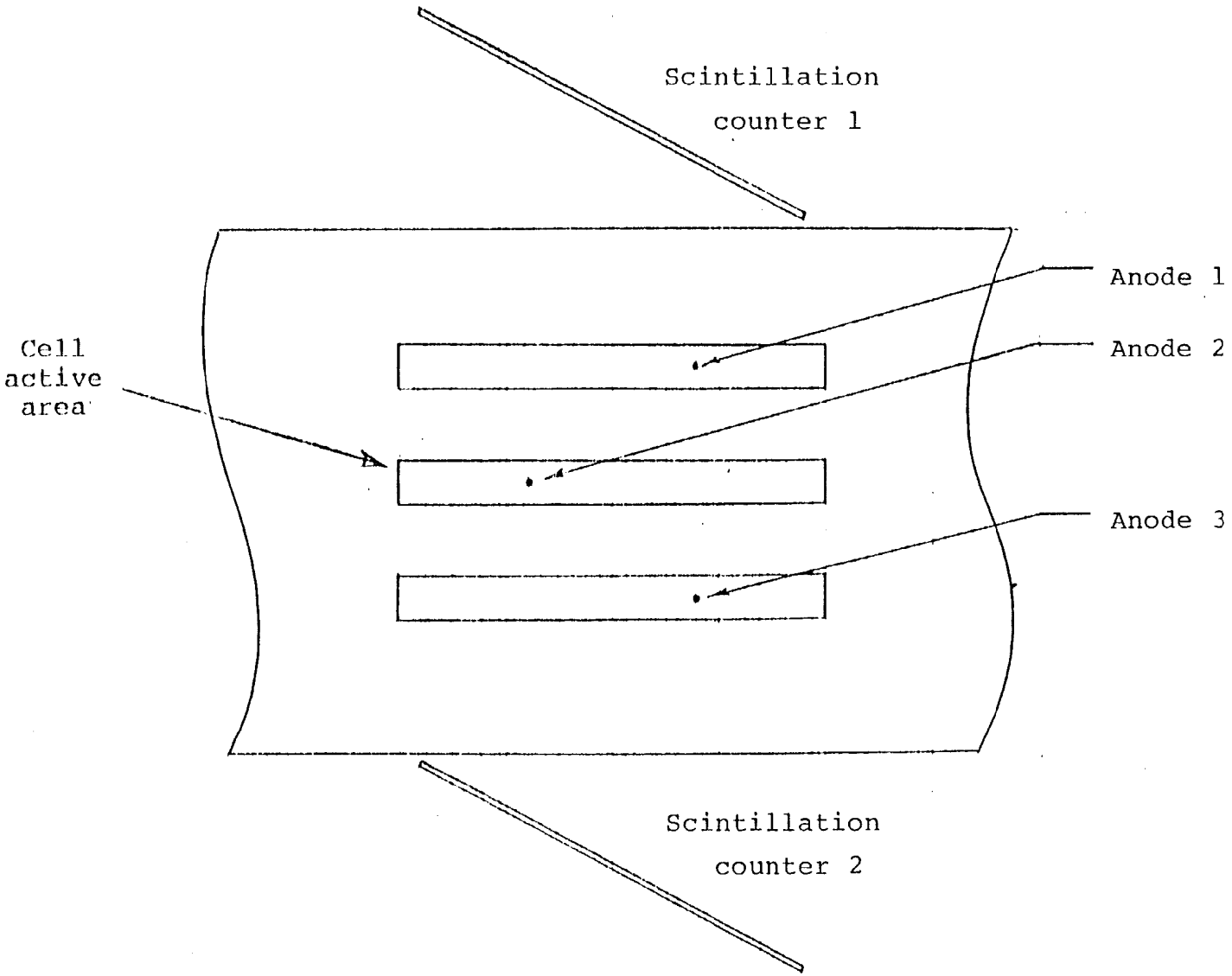

Figure 12.

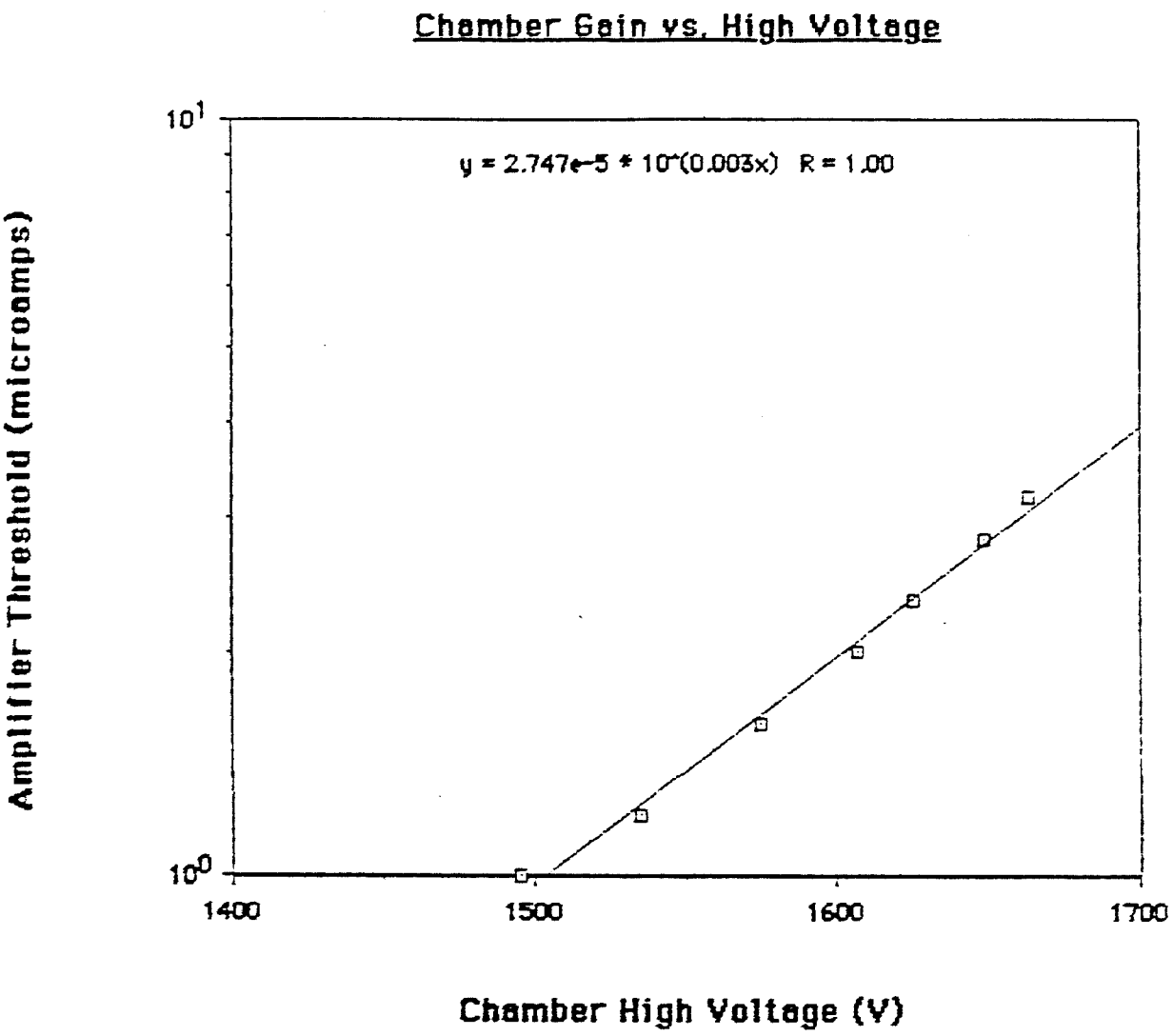
Chamber Gain vs. High Voltage
y = 2.747e-5 * 10^(0.003x) R = 1.00
10^1
10^0
1400
1500
1600
1700
Amplifier Threshold (microamps)
Chamber High Voltage (V)

Figure 13.

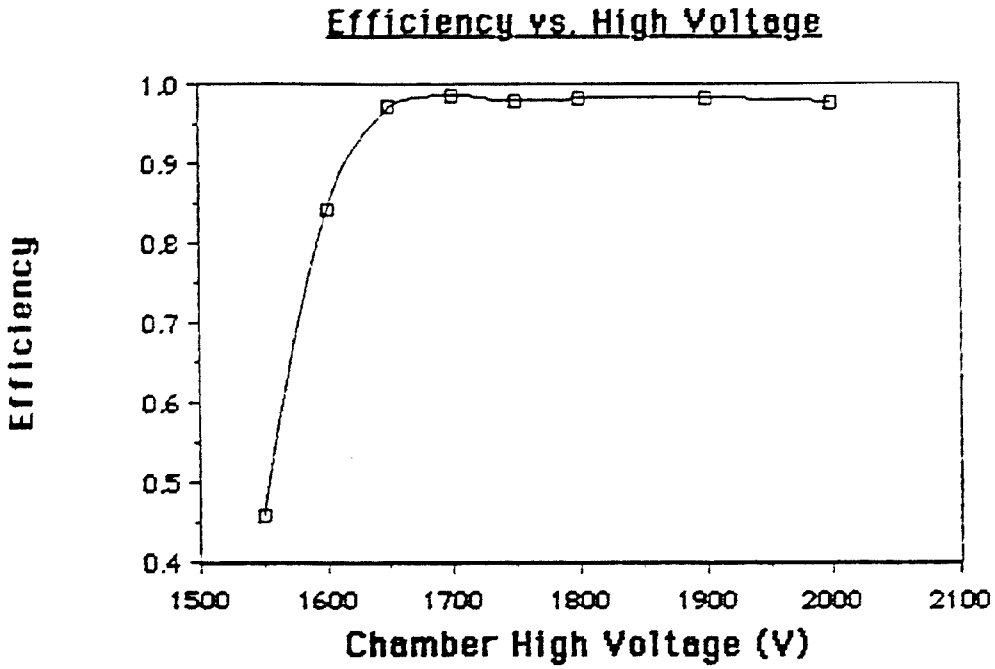
Efficiency vs. High Voltage
Efficiency
1.0
0.9
0.8
0.7
0.6
0.5
0.4
1500
1600
1700
1800
1900
2000
2100
Chamber High Voltage (V)

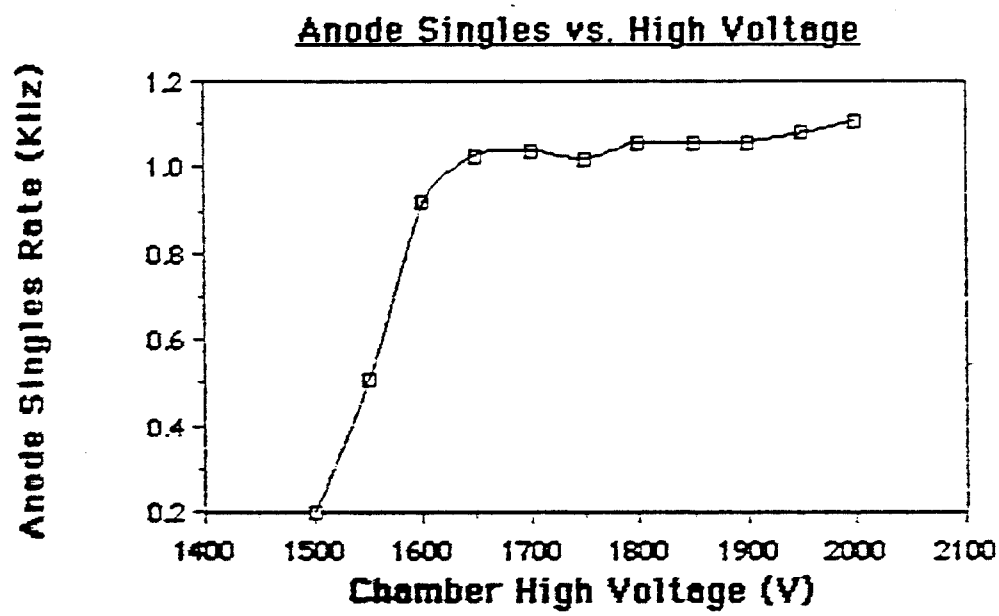
Anode Singles vs. High Voltage
Anode Singles Rate (KHz)
1.2
1.0
0.8
0.6
0.4
0.2
1400
1500
1600
1700
1800
1900
2000
2100
Chamber High Voltage (V)

Figure 14.

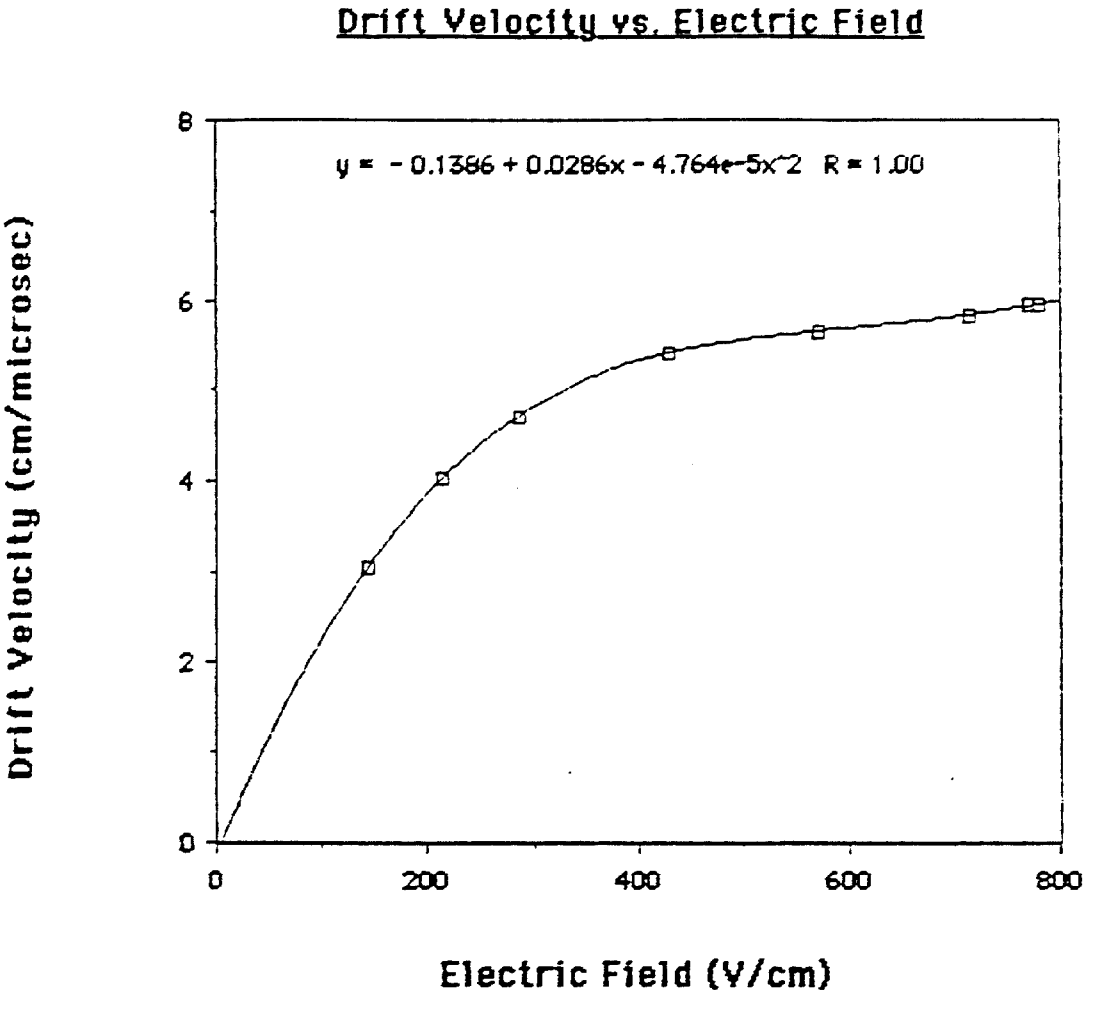
Drift Velocity vs. Electric Field
y = -0.1386 + 0.0286x - 4.764e-5x^2 R = 1.00
Drift Velocity (cm/microsec)
Electric Field (V/cm)
0
2
4
6
8
0
200
400
600
800

Figure 15. Drift time spectrum for an entire cell

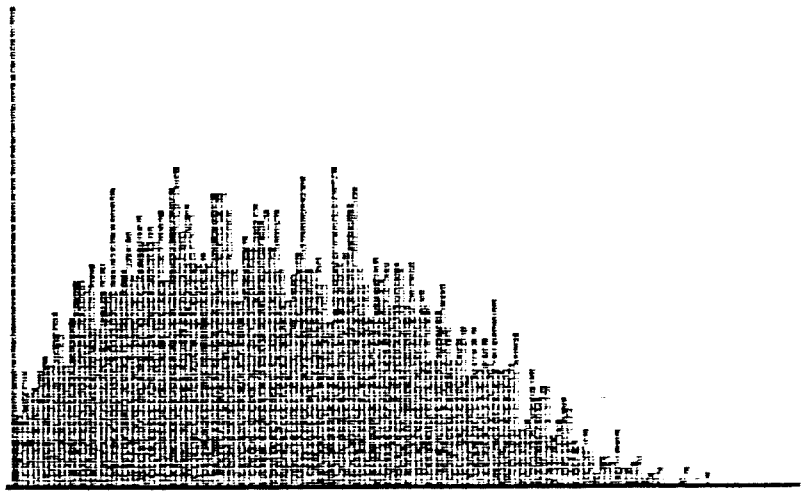

2.5ns/bin

Figure 16. Drift velocity in argon - ethane (linearity)

Figure 17. Drift velocity in argon - CO_2 (linearity)

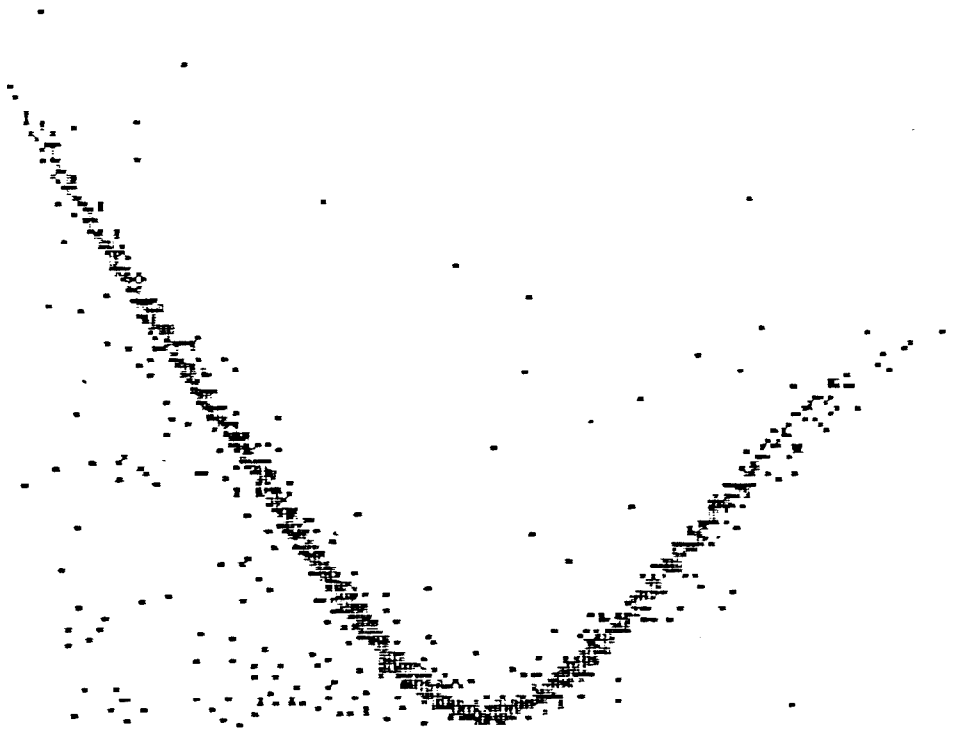

Figure 18. Global time resolution: cosmic rays through argon - ethane

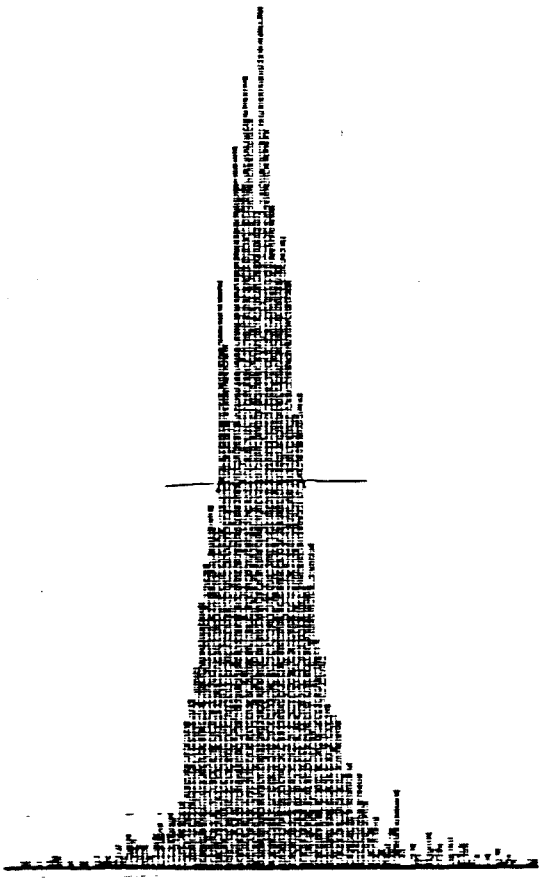

1.38ns/bin

Figure 19. Global time resolution: cosmic rays through argon - CO_2

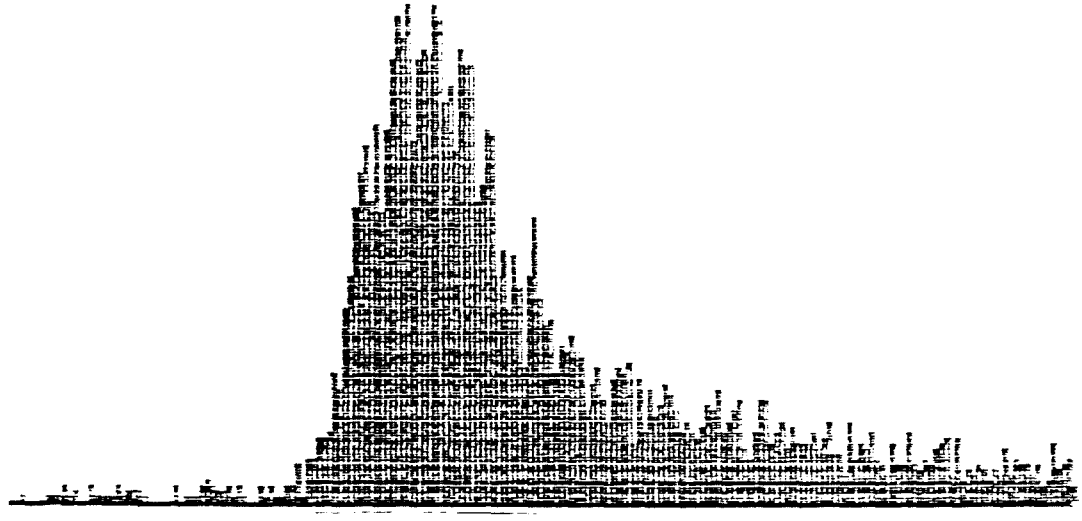

2.5ns/bin

Figure 20. Time resolution at one point: Ru106 tracks through argon - CO_2

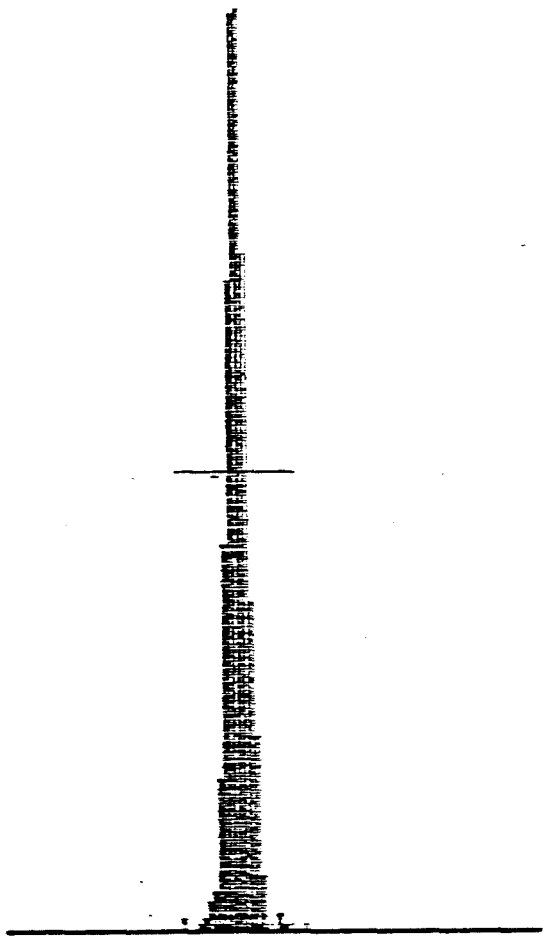

12.5ns/bin

Figure 21. Difference in Electron drift time vs. distance from midplane

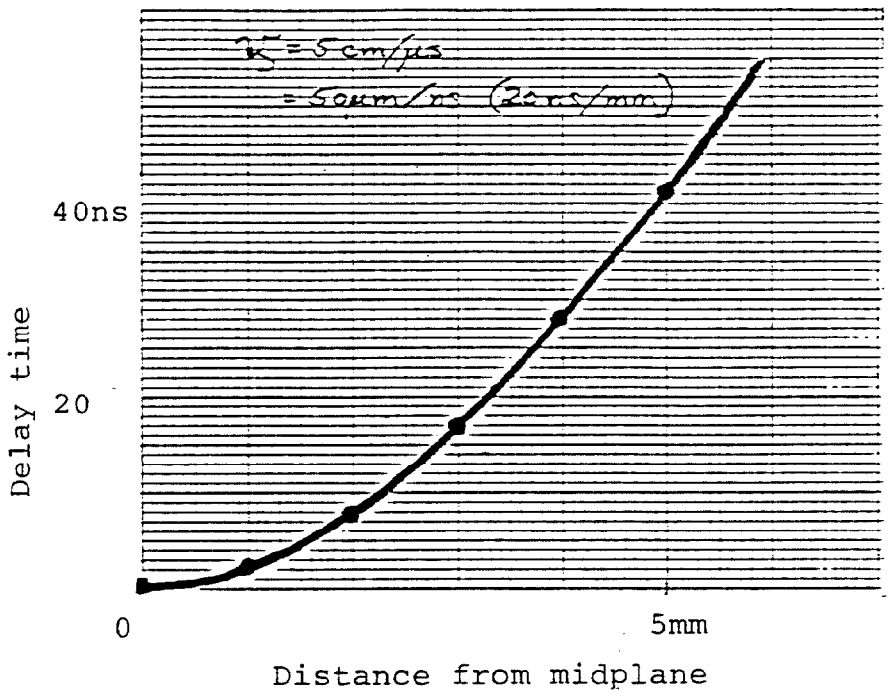

Fig 22

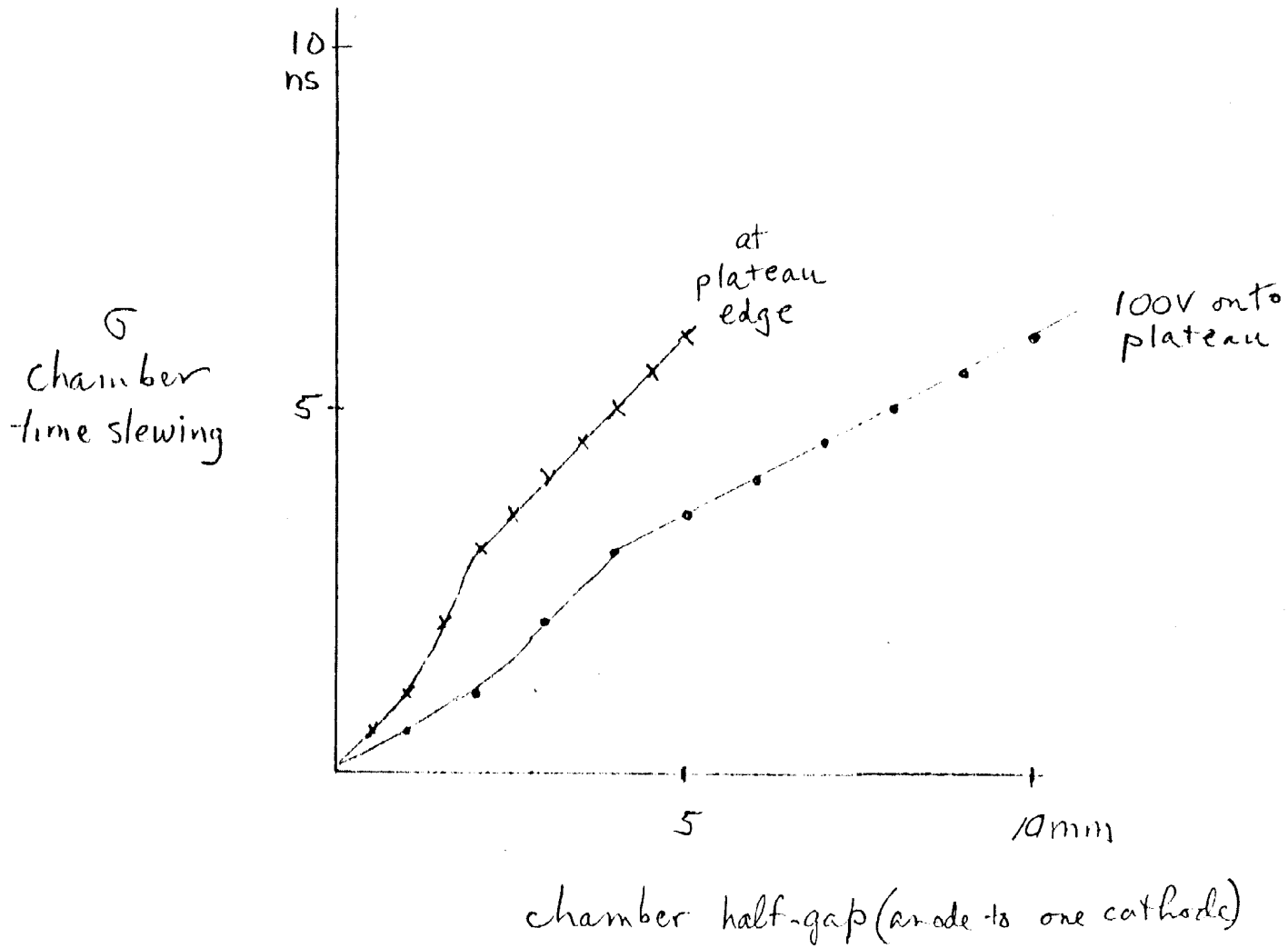
10
ns
5
σ
chamber
time slewing
at
plateau
edge
100V onto
plateau
5
10mm
chamber half-gap (anode to one cathode)